Solar and Greenhouse Gas Forcing and Climate Response in the Twentieth Century

GERALD A. MEEHL, WARREN M. WASHINGTON, T. M. L. WIGLEY, JULIE M. ARBLASTER, AND AIGUO DAI

National Center for Atmospheric Research, Boulder, Colorado*

(Manuscript received 6 September 2001, in final form 26 July 2002)

ABSTRACT

Ensemble experiments with a global coupled climate model are performed for the twentieth century with time-evolving solar, greenhouse gas, sulfate aerosol (direct effect), and ozone (tropospheric and stratospheric) forcing. Observed global warming in the twentieth century occurred in two periods, one in the early twentieth century from about the early 1900s to the 1940s, and one later in the century from, roughly, the late 1960s to the end of the century. The model's response requires the combination of solar and anthropogenic forcing to approximate the early twentieth-century warming, while the radiative forcing from increasing greenhouse gases is dominant for the response in the late twentieth century, confirming previous studies. Of particular interest here is the model's amplification of solar forcing when this acts in combination with anthropogenic forcing. This difference is traced to the fact that solar forcing is more spatially heterogeneous (i.e., acting most strongly in areas where sunlight reaches the surface) while greenhouse gas forcing is more spatially uniform. Consequently, solar forcing is subject to coupled regional feedbacks involving the combination of temperature gradients, circulation regimes, and clouds. The magnitude of these feedbacks depends on the climate's base state. Over relatively cloud-free oceanic regions in the subtropics, the enhanced solar forcing produces greater evaporation. More moisture then converges into the precipitation convergence zones, intensifying the regional monsoon and Hadley and Walker circulations, causing cloud reductions over the subtropical ocean regions, and, hence, more solar input. An additional response to solar forcing in northern summer is an enhancement of the meridional temperature gradients due to greater solar forcing over land regions that contribute to stronger West African and South Asian monsoons. Since the greenhouse gases are more spatially uniform, such regional circulation feedbacks are not as strong. These regional responses are most evident when the solar forcing occurs in concert with increased greenhouse gas forcing. The net effect of enhanced solar forcing in the early twentieth century is to produce larger solar-induced increases of tropical precipitation when calculated as a residual than for early century solar-only forcing, even though the size of the imposed solar forcing is the same. As a consequence, overall precipitation increases in the early twentieth century in the Asian monsoon regions are greater than late century increases, qualitatively consistent with observed trends in all-India rainfall. Similar effects occur in West Africa, the tropical Pacific, and the Southern Ocean tropical convergence zones.

1. Introduction

Warming of globally averaged surface temperatures has occurred in two periods in the twentieth century. The first was from the early 1900s to the 1940s, and the second from the late 1960s to the end of the century (Fig. 1b). Previous climate model experiments have suggested that the early twentieth-century warming could have been primarily due to ''natural'' forcings (mainly solar with some contribution from reduced volcanic activity), while the late twentieth-century warming was likely mainly due to increases of greenhouse gases (Cubasch et al. 1997; Wigley et al. 1997; Stott et al. 2000, 2001). However, inherent unforced variability could also play a role. In an experiment with increasing greenhouse gases but no solar or volcanic forcing, the early twentieth-century warming was simulated in one member of an ensemble mainly due to a warm phase of decadal variability in the Atlantic (Delworth and Knutson 2000). Thus, a combination of internal variability and external forcing could have contributed to the observed early twentieth-century warming.

Previous studies in the paleoclimate context suggest that during periods of enhanced solar forcing, there may be stronger tropical monsoon regimes (e.g., Kutzbach et al. 1998; Joussaume et al. 1999). However, these changes are due to orbital shifts that produce enhanced solar radiation in the northern Tropics in spring, not to an increase of total solar irradiance. Additionally, it has been shown in observations that a signature of enhanced solar forcing is evident in a warming of the upper tropical troposphere (van Loon and Shea 2000) and an intensified Hadley circulation implying stronger tropical

* The National Center for Atmospheric Research is sponsored by the National Science Foundation.

Corresponding author address: Dr. G. A. Meehl, NCAR, P.O. Box 3000, Boulder, CO 80307-3000.
E-mail: meehl@ncar.ucar.edu

precipitation (van Loon and Labitzke 1994; Labitzke and van Loon 1995). In this work, solar-related changes in ultraviolet (UV) were implicated as the cause.

Model experiments with solar forcing changes have been able to reproduce some aspects of these observations (Rind and Balachandran 1995; Haigh 1996; Balachandran et al. 1999; Rind et al. 1999; Shindell et al. 1999, 2001). Most of these studies included an hypothesized change of stratospheric ozone associated with the 11-yr solar cycle (related mostly to UV radiation). The enhanced UV radiation caused changes in the vertical gradients of temperature and wind that lead to altered planetary wave propagation and changes in circulation patterns in the lower stratosphere and upper troposphere. Though some of these studies note either direct (e.g., Balachandran et al. 1999) or implied (e.g., Rind and Balachandran 1995; Haigh 1996) changes in tropical precipitation with fluctuations of solar forcing, SSTs are usually fixed and there is no capability for coupled feedbacks at the surface to contribute to the response. Rind et al. (1999) used a slab nondynamic ocean in experiments comparing solar and greenhouse forcing. They conclude that there is little change in tropical precipitation due to solar forcing. In contrast, Balachandran et al. (1999) found that in a different model version there were small increases in tropical precipitation in response to increases in solar forcing.

The importance of ocean dynamical feedbacks in relation to solar forcing was pointed out by Waple et al. (2002). Such factors may lead to nonlinear responses of the climate system to solar forcing, and could help explain why solar forcing effects appear to be identifiable in observations over the past six centuries (Mann et al. 1998; Crowley 2000). Here, we will address the issue of nonlinearity using various combinations of forcings in a global coupled general circulation climate model.

Experiments with increasing greenhouse gases (GHGs) show that the infrared radiation (IR) forcing is relatively spatially uniform over land and ocean in all seasons. Thermal inertia and feedback effects, however, lead to strong warming differences, with land warming faster than ocean, and high-latitude amplification of warming due to ice–albedo feedback and a stable boundary layer (e.g., Cubasch et al. 2001). Such thermal contrasts should affect the strength of monsoon circulations, but the influences depend on the assumed anthropogenic forcings (Cubasch et al. 2001). Solar forcing differs fundamentally from anthropogenic forcing (which is mostly IR), since it is primarily shortwave forcing. Furthermore, solar forcing varies by season and geography, being greater in the Tropics in cloud-free areas during daytime. The response of the climate system to solar versus GHG forcing, therefore, could involve different coupled feedbacks at the surface and lead to different climate responses in transient climate change experiments. Indeed, some differences in climate response to these different forcings have already been noted (e.g., Shindell et al. 2001).

Early experiments with climate models showed comparable climate system responses to increased CO_2 and enhanced solar forcing (Wetherald and Manabe 1975; Hansen et al. 1984). However, those were equilibrium experiments with nondynamic oceans. Some later modeling studies cited above examined climate response to 11-yr solar irradiance changes. In this paper we examine the lower-frequency (multidecadal) transient climate system response of a global coupled climate model. We first analyze multimember ensembles forced with increases in GHGs and tropospheric ozone, decreases in stratospheric ozone, and increasing sulfate aerosol direct effect. We then contrast these results with a multimember ensemble of those forcings in combination with solar forcing. Additionally, the linearity issue is addressed by comparing the differential results of the above two cases with a multimember ensemble of model integrations performed with only solar forcing. Our goal is to identify differences in the nature of the early and late twentieth-century forcings and responses simulated by the model. We hypothesize that due to the different nature of the forcing (shortwave for solar, and IR for GHGs), the transient response of the climate system could be different, with solar forcing producing relatively warmer tropical areas and stronger tropical precipitation regimes.

As noted above, it has been suggested that a significant part of solar forcing of the climate system is related to the UV part of the solar spectrum, and that this influence could be greatest in the stratosphere especially with regards to effects involving ozone (e.g., Rind et al. 1999). A notable caveat to the analyses here is that the solar forcing is manifest only as changes in total solar irradiance, with no wavelength dependence of the solar forcing in the model (changes in solar forcing are simply total solar irradiance anomalies added to the solar constant). Additionally there is no response of stratospheric ozone to fluctuations of incoming solar radiation, and the atmospheric model does not have a well-resolved stratosphere. We will show that the climate responses in this model occur in the troposphere mainly due to coupled land–atmosphere–ocean interactions.

Results are shown for the average of the ensemble members and differences for early (1936–45 minus 1900–09) and late (1990–99 minus 1961–70) century periods. These differences are assessed in two ways. First, as a measure of consistency of response across the ensemble members, we calculate a signal-to-noise measure (the ensemble mean divided by the intraensemble standard deviation). If this value is greater than 1.0, we judge the results to be consistent across ensemble members (e.g., Cubasch et al. 2001). As a measure of the relative magnitude of the differences in comparison to internal model variability, we calculate a t statistic using a 50-yr period from the control integration (as-

suming equality of variances) to determine if the differences exceed model internal variability.

2. The model and experiments

The model used in the experiments is the Parallel Climate Model (PCM), a fully coupled global ocean–atmosphere–sea ice–land surface model that produces a stable climate without flux adjustment (Washington et al. 2000). The atmospheric component is the National Center for Atmospheric Research (NCAR) Community Climate Model version 3 (CCM3) with T42 resolution (an equivalent latitude–longitude grid spacing of roughly 2.8° × 2.8°) and 18 levels (hybrid coordinates; see details and references in Kiehl et al. 1998). The land surface component is the Land Surface Model (LSM), with specified vegetation types and a comprehensive treatment of surface processes (see Bonan 1998). The CCM3 has a relatively low equilibrium climate sensitivity for a doubling of CO_2 of 2.1°C when coupled to a slab ocean with implied ocean heat transports, sometimes called a ''*q*-flux'' ocean (Meehl et al. 2000). The sensitivity is at the low end of model responses to increasing CO_2 (Cubasch et al. 2001). This is likely due in part to the model's low ice-albedo feedback (in turn, related to cloud changes), which also involves ocean heat transport changes in the high latitudes (Meehl et al. 2000).

The PCM ocean component is a version of the Parallel Ocean Program (POP) with 32 levels in the vertical and 0.67° nominal latitude–longitude resolution reducing to 0.5° in latitude in the Tropics (actual longitudinal grid spacing in the equatorial Pacific ranges from about 0.6° in the east to 0.9° in the west due to the effects of the rotated Pole over northern North America). El Niño amplitude is comparable to observations (Meehl et al. 2001). Sea ice is thermodynamic with elastic–viscous–plastic (EVP) dynamics as described by Washington et al. (2000).

After spinup to 1870 conditions (see details in Washington et al. 2000), an ensemble of five experiments, each starting from a different initial state in the control run at least 20 years apart, is run with time-evolving greenhouse gases, sulfate aerosol (direct effect only; black carbon not included), and stratospheric and tropospheric ozone changes. Sulfate loadings are taken from runs with NCAR's Climate System Model (CSM) that has interactive sulfur chemistry allowing direct input of SO_2 emissions. This experiment is referred to as ''GHG + sulfates.'' The forcing is shown in Fig. 1a. Tropospheric ozone increases gradually throughout the twentieth century, while stratospheric ozone begins decreasing in 1970. Further details regarding the forcing are described in Dai et al. (2001b). Results from the GHG + sulfates experiments are shown in Dai et al. (2001a,c).

A second set of four experiments with varying initial conditions is run with the addition of the time-evolving solar forcing from Hoyt and Schatten (1993; corrected and updated) to the GHG + sulfate forcing. This solar forcing dataset is derived from a composite solar irradiance model based on five solar indices plus an added activity component. The five indices are solar cycle length, cycle decay rate, mean level of solar activity, solar rotation, and fraction of penumbral sunspots. For 1979–92, the irradiances are scaled to the mean *Nimbus-7* measurements. The ensemble mean of the GHG + sulfates is subtracted from these experiments to obtain the solar response as a residual, referred to as ''solar residual.'' A third set of four experiments is run with just the time-varying changes of solar forcing from Hoyt and Schatten (1993), and is referred to as ''solar-only.''

Another plausible solar forcing dataset is Lean et al. (1995). Theirs is a reconstruction of solar total irradiance that includes a separately determined 11-yr activity cycle and a longer-term component based on the average amplitude of each sunspot cycle. Stott et al. (2001) discuss the differences for their model experiments of these

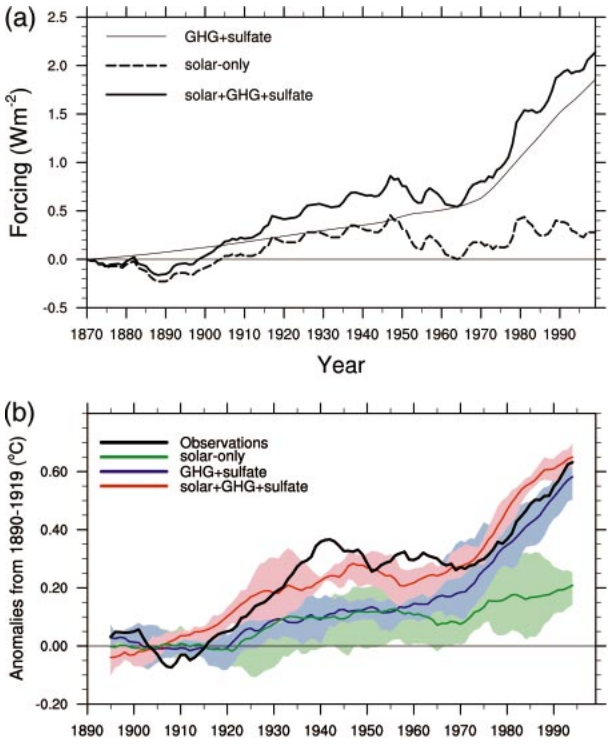

FIG. 1. (a) Time series of the top of the troposphere radiative forcing from the coupled model for GHG + sulfates (thin solid line), solar forcing (dashed line) from Hoyt and Schatten (1993), and the sum of the thin solid and dashed lines, the thick solid line, is solar + GHG + sulfates. (b) Global annual mean surface air temperature, 11-yr running mean (central value plotted, so the average of, e.g., 1 Jan 1895–31 Dec 1905, is plotted at 1 Jul 1900), for observations (black line; Jones et al. 1999), ensemble mean (blue line) and range (defined as the max and min for any member of the ensemble for a given year, shading) for GHG + sulfates experiments from coupled model; ensemble mean (red line) and range (shading) for solar + GHG + sulfates experiments from coupled model; ensemble mean (green line) and range (shading) for solar-only experiments.

two solar forcing datasets. The Lean et al. data show a more gradual increase of the solar forcing in the early twentieth century compared to Hoyt and Schatten, with a later maximum. The Hoyt and Schatten forcing provides a closer fit of the model response to the observed maximum of warming that occurred in the 1940s (Stott et al. 2001; Smith et al. 2003). Regarding the discrepancies between the two forcing datasets, Lean and Rind (1998) conclude, ''These differences, which cannot be resolved without improved understanding of the solar origins of the variations, reflect the large uncertainties in reconstructing historical solar irradiances from a limited solar monitoring database, with only rudimentary knowledge of the pertinent physical processes.''

Such differences between the solar forcing datasets, important for a detection/attribution study, are less crucial in the present paper since we are focusing on forcing/response aspects. In other words, we are interested in the response to a given amount of solar forcing, not the forcing history. It is the mechanisms of the response that are the focus of this paper, and these should be comparable with either solar forcing dataset.

The total top-of-troposphere forcing for solar + GHG + sulfate + ozone, as well as the GHG + sulfates and the solar-only are shown in Fig. 1a. For GHG + sulfate, positive radiative forcing (relative to the year 1870) increases steadily to a value of about $+0.5$ W m^{-2} around 1970, and then increases in the late century by about an additional 1.3 W m^{-2} to end up around $+1.8$ W m^{-2} at the year 2000. The solar forcing (relative to its 1870 value; anomalies divided by 4 to account for spherical geometry, and multiplied by 0.7 to account for planetary albedo) increases to a relative maximum in the mid-1940s of over $+0.4$ W m^{-2}, decreases, and then increases again to late century maximum values of about $+0.4$ to $+0.5$ W m^{-2}. Thus the early century solar forcing is about a factor of 3 less than the late century GHG + sulfate forcing increment. In comparing the two periods, if ocean lag effects were similar and if the system were linear, the early century response due to solar forcing should be about a third the size of the late century response due to increased GHGs. Of interest here, however, are possible nonlinearities that we address by testing the additivity of solar and GHG + sulfates responses. (Note that differential lag effects are essentially linear and additive, so that a breakdown of additivity points toward nonlinear mechanisms.) To test additivity, the difference of solar + GHG + sulfate minus GHG + sulfate will be compared to the solar forcing alone ensemble.

3. Changes in surface temperature

Figure 1b shows the globally annually averaged surface air temperature from observations [the solid black line is the 11-yr running mean used by the Intergovernmental Panel on Climate Change (IPCC); e.g., Jones et al. 1999], along with the model responses (11-yr running mean) to the forcings in Fig. 1a. The ranges of the ensemble members are depicted by the shading. The range is defined here as the maximum and minimum of any member of the ensemble for a given 11-yr mean. Results from the GHG + sulfate experiments in Fig. 1b are described more fully in Dai et al. (2001a).

The GHG + sulfate ensemble mean is colder than the solar + GHG + sulfate ensemble mean due to less positive radiative forcing in the former compared to the latter (Fig. 1a). The GHG + sulfate ensemble mean warms somewhat in early century (0.08°C from an 11-yr ensemble mean centered on 1905, to one centered on 1940), but does not show evidence of the large early century warming seen in the observations. The addition of solar forcing produces warming (0.24°C) closer to the observed during that time period, consistent with previous studies mentioned above. The range of responses from the solar + GHG + sulfate ensembles is about 0.05°–0.10°C.

The solar-only ensemble mean trend is similar to the GHG + sulfate ensemble mean up to the 1950s, with warming in both experiments of around 0.1°C. When the forcings are added, they produce a larger early century warming closer to observed. The late century (from the 11-yr period centered on 1965, to the one centered on 1995) solar-only ensemble shows warming of about 0.1°C. To get the rapid rate of warming seen in the observations requires the additional forcing from the GHG + sulfates (about 0.4°C).

Overall, the time series from GHG + sulfates + solar shows reasonable agreement with the observations during the course of the twentieth century. The most marked discrepancy is that the model warms too little in the early century. Clearly there are many issues involved with such a comparison in a climate change detection/attribution sense, such as model sensitivity, uncertainties in the magnitude of the forcings, other forcings not included in these experiments, and differences between the internally generated variability in the model and that realized in the observations. We will not consider the detection/attribution issue, but will focus on the nature and mechanisms of the coupled climate response to these different forcings.

One of the reasons why the early century warming for the solar + GHG + sulfate ensemble is less than the observations could be our neglect of volcanic aerosols. The addition of volcanic aerosols improves the quantitative comparison of the model experiments with observations, and their inclusion, along with solar forcing, has been shown to contribute substantially to the early century warming (e.g., Stott et al. 2000; Ammann et al. 2002, manuscript submitted to *Geophys. Res. Lett.*, Meehl et al. 2002, manuscript submitted to *Geophys. Res. Lett.*) though the solar forcing added to the GHG + sulfates accounts for much of the early century warming. However, in a previous modeling study one member of a 5-member twentieth-century climate simulation ensemble without solar forcing produced early century

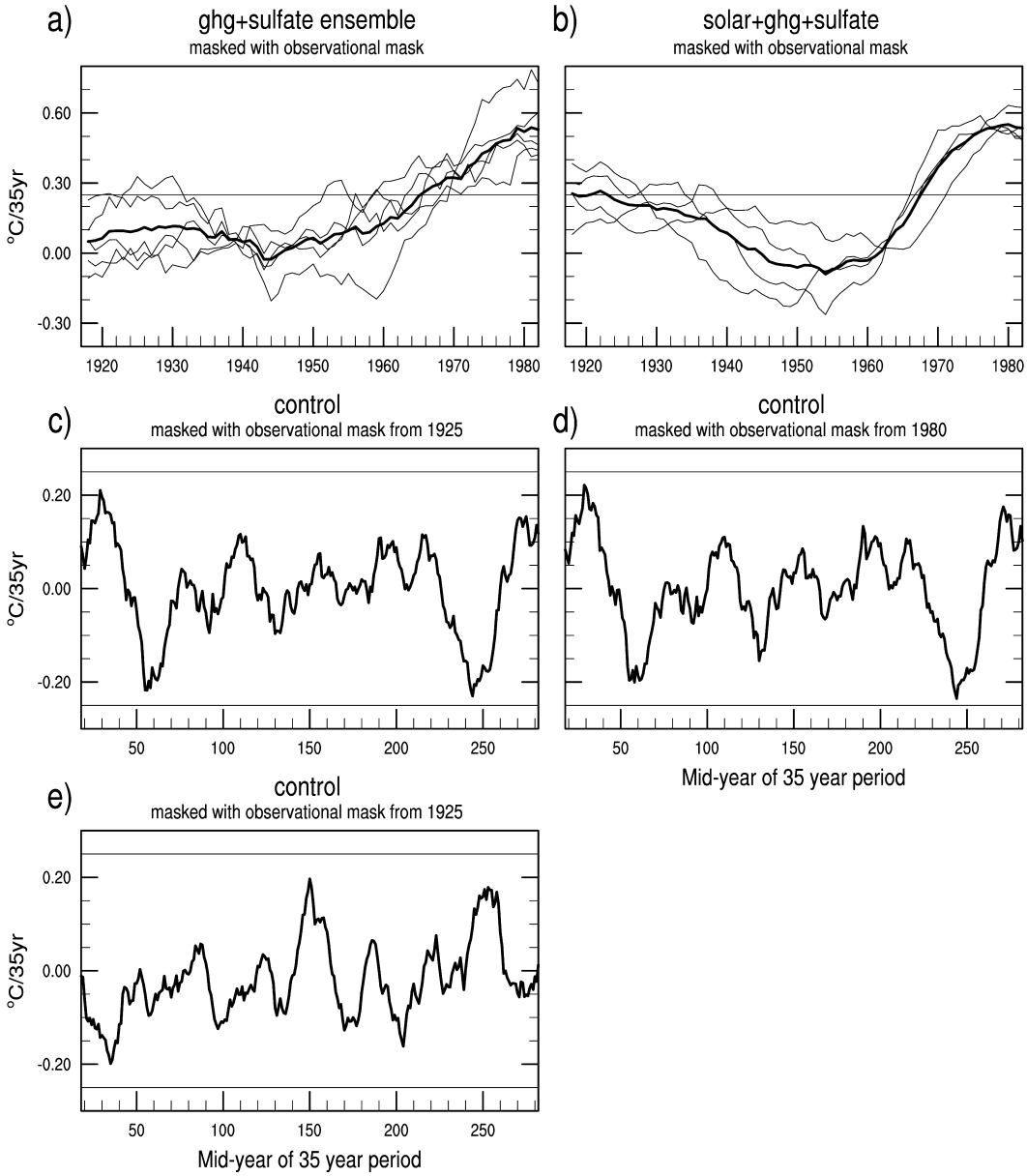

FIG. 2. (a) Time series of 35-yr globally averaged surface air temperature linear trends (plotted at 35-yr midpoints, first 35-yr segment begins at 1900) from the GHG + sulfate ensemble mean (thick solid line), and individual ensemble members (thin lines); (b) same as (a) but for the solar + GHG + sulfate ensemble mean; (c) a similar calculation from the 300-yr control run with perpetual 1992 forcing using the observational mask from 1925 representing the early century; (d) the same calculation and control run as in (c) but using the mask from 1980 representing the late century; (e) the same calculation as in (c) but using the 300-yr perpetual 1870 control run with the 1925 observational mask. Horizontal lines indicating trend values of either +0.25 and −0.25 are included to relate to the magnitude of the ensemble mean early twentieth-century trend values in (b).

temperature trends comparable to observations with just GHG + sulfates (Delworth and Knutson 2000).

To address the likelihood that such early century temperature trends could occur due to natural unforced internal low-frequency variability, or require either GHG + sulfates or solar forcing, we analyze two 300-yr control runs by applying a moving 35-yr linear trend calculation yielding 265 trend calculations for each of the control runs. First, we analyze the 300-yr control run with perpetual 1992 forcing using the observational mask from 1925 representing the early century (Fig. 2c) and the mask from 1980 representing the late century (Fig. 2d). At no time in the model control run does an unforced 35-yr trend ever reach 0.25°C as in the early century model ensemble mean for solar + GHG + sulfate in Fig. 2b. One of the ensemble member 35-yr early

century trends in Fig. 2b reaches 0.4°C. The largest 35-yr trends from the unforced control run are +0.22° and −0.23°C. The 35-yr trends of greater than 0.20°C only occur for 7 out of the 265 periods calculated for the 1925 mask, and 6 out of 265 periods computed for the 1980 mask. For the perpetual 1870 control run in Fig. 2e shown for the 1925 mask, no 35-yr trend exceeds 0.20°C. Meanwhile, all ensemble members for the late twentieth century for solar + GHG + sulfates and GHG + sulfates exceed 35-yr trends of 0.25°C, with one member of the GHG + sulfates ensemble reaching nearly 0.8°C in Fig. 2a.

Comparing the 35-yr early century temperature trends from the GHG + sulfates and solar + GHG + sulfates, the former shows ensemble mean early twentieth-century 35-yr trends of about 0.1°C, while the latter are about 0.25°C. However, two members of the GHG + sulfates ensemble in Fig. 2a equal or exceed the ensemble mean for the solar + GHG + sulfates in Fig. 2b, suggesting that relatively large early century temperature trends, comparable to those produced by the addition of solar forcing, can be produced by the GHG + sulfates forcing alone as in the Delworth and Knutson study. However, comparison of the spread of the ensemble members in Figs. 2a and 2b shows that the addition of solar forcing produces consistently large early twentieth-century temperature trends compared to GHG + sulfates alone. Thus, while it is possible that solar forcing is not necessary to produce enhanced early century warming with GHG + sulfates in the model, the addition of solar forcing produces a more consistent early twentieth-century warming. The mechanism of this warming will be addressed shortly.

Annual 10-yr running mean zonal surface air temperature anomalies (no observational mask is applied) relative to 1961–90 are shown in Fig. 3a for the solar + GHG + sulfate ensemble mean. The model ensemble shows a relative warming in the late 1940s that is largest at high latitudes of the Northern Hemisphere with values of nearly +0.2°C (Delworth and Knutson 2000). Warming appears again around 1980 at all latitudes, but is largest at high northern latitudes. This amplification is mainly due to the effects of ice-albedo feedback (Meehl et al. 2000). For the GHG + sulfate ensemble (using 10 members in this case; Fig. 3b), warming only occurs in the late twentieth century as could be expected from Fig. 1b.

To see the effects of the model response to solar forcing compared to GHG + sulfate, the difference of solar + GHG + sulfate minus GHG + sulfate (solar residual) is shown in Fig. 3c. The increased global-mean warming arising from solar forcing (Fig. 1b) is manifest most markedly at high latitudes of the Northern Hemisphere associated with ice-albedo feedback, with maximum values of about +0.7°C north of 65°N in the late 1940s. Contributions in the Tropics and at high southern latitudes are about +0.1°–+0.2°C. The contribution of the solar forcing to the late twentieth-century warming is again most notable at high northern latitudes between 1985 and 1995 with values of about +0.3°C north of 70°N. The high-latitude warming associated with ice-albedo feedback was noted in the earlier studies with increased solar forcing (e.g., Wetherald and Manabe 1975). Though the impact of sulfate aerosols is greatest in the northern midlatitudes where the emissions are largest (e.g., Kiehl and Briegleb 1993; Meehl et al. 1996), warming is only slightly decreased there in Fig. 3b. The effects of the well-mixed ocean and the consequently large thermal inertia inhibit high-latitude warming in the circumpolar southern regions (e.g., Cubasch et al. 2001).

There is lower-amplitude warming in the Tropics (up to +0.1°C in Fig. 3c), but with a closer correspondence to the time evolution of the global mean in Fig. 1b with maximum relative values from about the mid-1930s until the late 1950s. Thus, warming at lower latitudes appears to precede high-latitude amplification. This suggests an important role of tropical processes in the climate system response to external forcing.

4. Seasonal changes in forcing and response

It was noted earlier that the spatial and seasonal patterns of solar (shortwave) forcing and GHG (longwave) forcing are different, and that solar forcing shows strong spatial differentiation and a stronger land–ocean contrast. We then hypothesized that this might lead to relatively greater changes in tropical precipitation for solar forcing, given the same global-mean, annual-mean magnitudes for solar and GHG forcing. We now explore this hypothesis further.

Figures 4 and 5 show early and late century differences in net solar absorbed and net IR at the surface (downward is positive in both cases, indicating more energy entering the surface), and total cloud for December–January–February (DJF) and June–July–August (JJA) at all grid points (global), land grid points, and ocean grid points (the latter includes sea ice points as well). The plots show ensemble means (boxes), values for each ensemble member (dots), together with the intraensemble standard deviation (bars). Results are shown for solar-only forcing and GHG + sulfates forcing in the early century in Fig. 4. Figure 5 shows early century solar residual (solar + GHG + sulfates minus GHG + sulfates, which should be comparable to the solar-only cases in Fig. 4) and late century GHG + sulfates.

All else being equal, one might expect an increase in solar irradiance to result in an increase of net solar absorbed at the surface. However, this is not the case for the solar-only ensembles in Fig. 4a. The global change in net solar absorbed is near zero for the ensemble mean, with small increases over the ocean (+0.16 W m^{-2} in DJF, +0.07 W m^{-2} in JJA) offset by small decreases over land (−0.20, −0.10 W m^{-2}). These changes are less than half the intraensemble standard deviations,

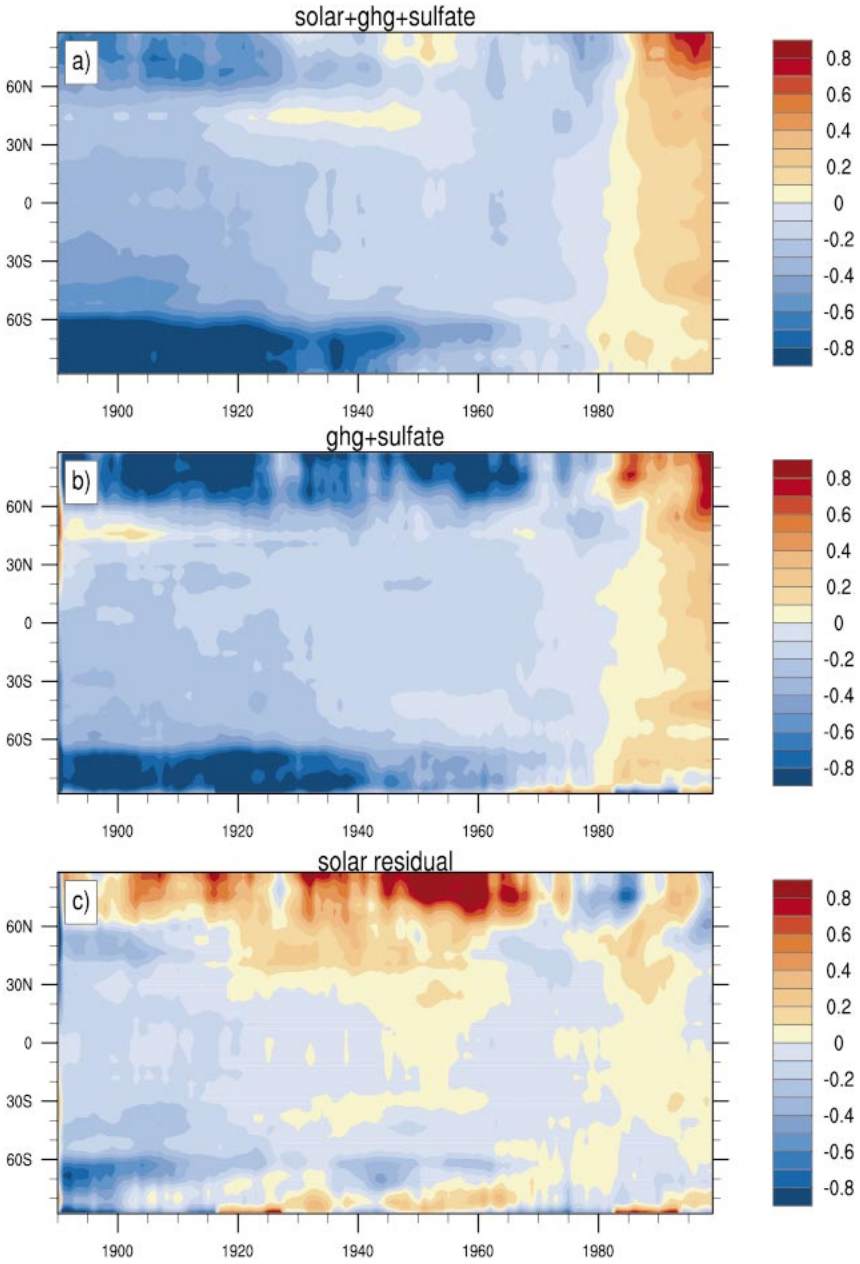

FIG. 3. (a) Annual 10-yr running mean zonal surface temperature anomalies (no observational mask is applied) relative to 1961–90 for the solar + GHG + sulfate ensemble mean. The 10-yr running mean differences are plotted not at the midpoint of the 10-yr average but at the tenth year as in Delworth and Knutson (2000); (b) same as (a) except for the GHG + sulfate ensemble (10 members); (c) same as (a) except for the difference of (a) minus (b).

(except for DJF over the ocean), as well as less than half the natural variability standard deviations from a 50-yr segment (roughly corresponding to the half-century time period being analyzed) of the control run. The negative changes over land are associated with increases in cloud (Fig. 4c). Over ocean, changes in absorbed solar radiation are not so clearly related to cloud changes. In any event, the cloud changes are small, mostly less than half the intraensemble standard deviation.

For the early century GHG + sulfate ensemble mean changes, global, land, and ocean gridpoint averages all show decreases in net solar radiation (Fig. 4a). However, the changes are either comparable to, or less than, the intraensemble standard deviations. Changes are larger in JJA, and (as for solar forcing) there appears to be a link to cloud changes over land in this season (reduced shortwave flux going with increased cloud).

For net infrared changes in Fig. 4b, GHG + sulfate

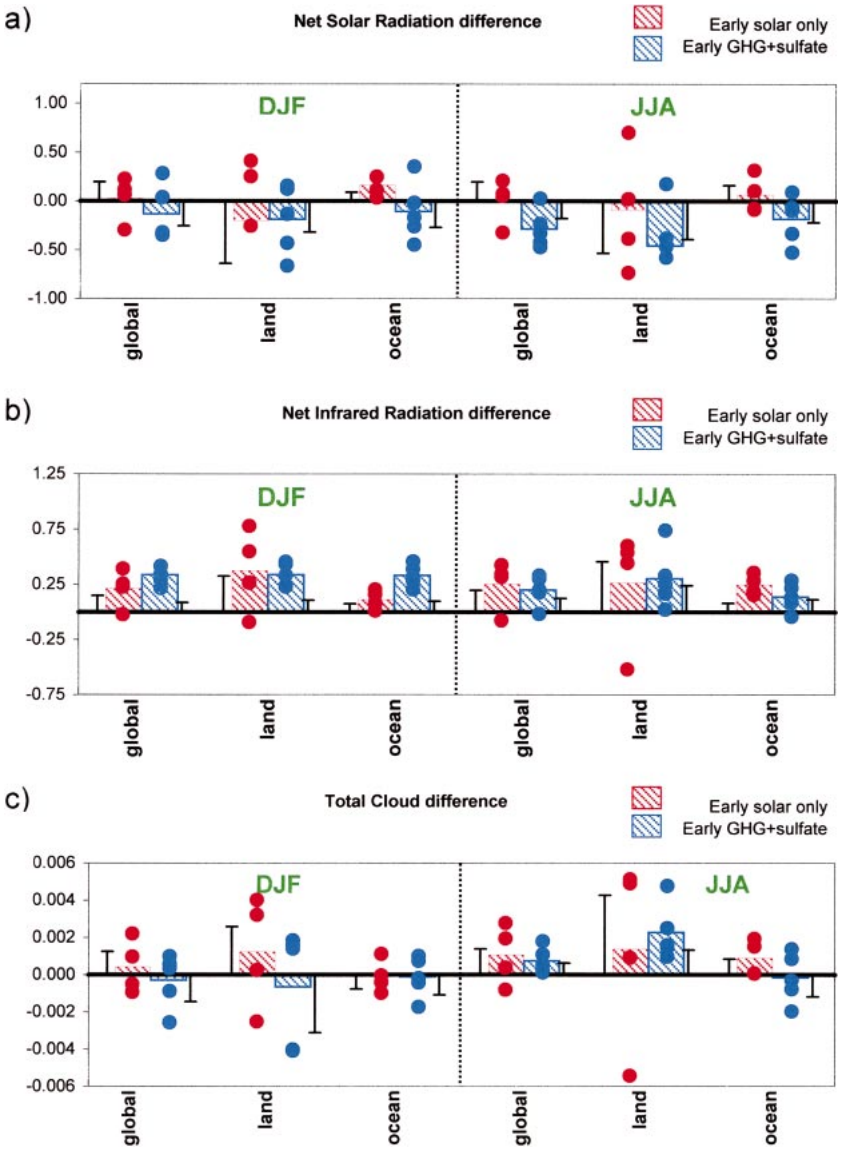

FIG. 4. (a) DJF and JJA differences for net solar radiation for global, land, and ocean area averages for the early century solar-only and the early century GHG + sulfates (W m^{-2}); (b) same as (a) except for net IR differences; (c) same as (a) except for total cloud differences (cloud fraction). Boxes indicate ensemble mean differences, dots are the individual values from each ensemble member (dots may overlap in some cases if ensemble member values are the same), and black bars indicate one intraensemble std dev. Std dev bars are plotted in the same direction as ensemble mean changes for convenience.

forcing should show increased infrared radiation into the surface (because CO_2 has increased and there is more water vapor evaporating from the warmer ocean surface). This is indeed the case for both seasons and for global, land, and ocean averages. Differences in JJA are near one standard deviation of intraensemble and natural variability standard deviation. There is much more consistency with the ensemble mean in DJF. Interestingly, for the solar-only ensemble means, there is a similar response to the GHG + sulfate for the early century with global, land, and ocean averages all showing an increase of infrared energy into the surface. For the GHG + sulfate case (as noted above), the increase of net infrared is both direct (due to more CO_2 and greenhouse gases) as well as indirect (due to more water vapor as the system warms and evaporation increases). For the case of increased solar radiation, the IR increases are all indirect; the ocean warms enough to increase evaporation, water vapor, and clouds over both land and ocean. These changes, however, are all small and not particularly consistent across ensemble members.

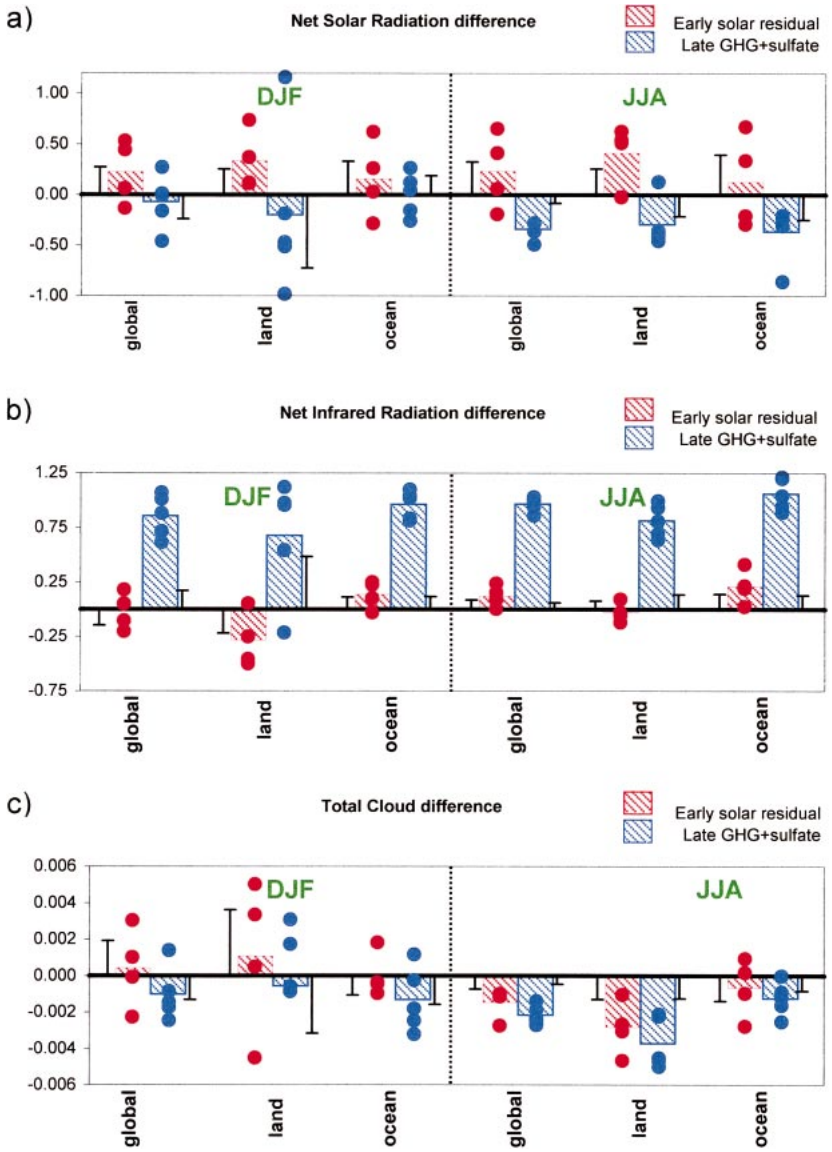

FIG. 5. Same as Fig. 4 except for the early century solar-residual and the late century GHG + sulfates.

In Fig. 5a, there is a different response when the solar forcing is calculated as a residual in the GHG + sulfate + solar ensembles (cf. red boxes in Fig. 5a with those in Fig. 4a). Now there are increases in global, land, and ocean net solar radiation at the surface for DJF and JJA and the changes are much larger in magnitude than for the solar-only case. The land differences for DJF and JJA exceed one standard deviation of the intraensemble standard deviations indicating a consistent response across the ensembles, while the global values are just less than 1.0 for that ratio. These changes in net solar are associated with consistent decreases in cloud over global, land, and ocean areas in JJA (Fig. 5c). In DJF, however, there is no clear link to cloud changes.

Land–ocean differentials are also quite different when the solar-only and solar-residual cases are compared. In JJA in the solar-residual case, the net solar radiation increase over land (0.41 W m^{-2} with a ratio to the intraensemble standard deviation of 1.55) is much larger than the increase over the ocean areas (0.13 W m^{-2}). In the solar-only case, the corresponding solar radiation changes are -0.10 over land versus $+0.07$ W m^{-2} over the ocean. This suggests that the increased solar input over land areas in the solar-residual case could contribute to enhanced land–sea temperature gradients and stronger monsoons relative to the solar-only case. This will be addressed further below.

These differential shortwave effects are not echoed

in the JJA IR results. For solar-only (Fig. 4b), land changes are slightly greater than the ocean changes (0.27 versus 0.25 W m^{-2}). For solar-residual (Fig. 5b), ocean changes are much greater than over land (0.21 versus -0.03 W m^{-2}). In terms of total flux differentials, however, the shortwave results dominate. For the solar-residual case, the increase over land is about 30% greater than over the ocean. For the solar-only case the increase over land is only about one-quarter that over the ocean. The monsoon implications for total flux changes are, therefore, the same as those for shortwave changes.

Figures 4 and 5 also allow us to compare early and late century GHG + sulfate responses. For the late century versus early century GHG + sulfate, larger increases in net infrared energy into the surface should be expected due to the greater increase of GHGs and more water vapor evaporating from the warmer surface. This is indeed the case for both seasons and all areas if the blue boxes in Figs. 5b and 5a are compared. Relative to both the intraensemble and natural variability standard deviations, the late century changes are highly significant. These changes are clearly associated with decreases in cloud amount (Fig. 5c). In the early century period, IR fluxes and cloud changes are not strongly related, perhaps reflecting lower signal-to-noise ratios.

For shortwave changes, signal-to-noise ratios are relatively low for both time periods. The changes are also of similar magnitude in both periods, with net decreases in both seasons and over land and ocean. In the early century period, there is no clear relationship between cloud and shortwave flux changes. In the late century period, reduced fluxes are apparently associated with reduced cloud amounts. IR effects dominate in the late century, while in the early century, IR effects are more important only in DJF.

It is apparent from comparing Figs. 4 and 5 that, for the early century period, the climate system response to solar-only forcing differs from that of solar forcing occurring in conjunction with GHG + sulfate forcing. The main differences are in net fluxes over land. In both seasons, the solar-residual results show an increase in solar flux relative to the solar-only results of around 0.5 W m^{-2}. In DJF, this is more than offset by the differential IR fluxes. Here it is the solar-only results that show an increase relative to the solar-residual results. In JJA, however, while the IR flux differences partly offset the shortwave differences, the net effect is a greater flux for the solar-residual cases. Thus, in JJA, the solar-residual has a larger land forcing contrast than does solar only. If this effect, averaged over all land and ocean areas in Figs. 4 and 5, is also a feature of land–ocean contrasts in monsoon areas, one might expect monsoon responses in the solar-residual case to differ from those in the solar-only case. These differential forcing changes, while not always significant relative to intraensemble or interannual variability, may well be a manifestation of nonlinear behavior in the model.

To examine these ideas further, we need to be more geographically specific and investigate changes in radiation fluxes and precipitation for tropical areas. We do this in the next section.

5. Geographical changes in response

Here, we consider two issues: differences between responses to shortwave and longwave forcing, and differences between solar responses in isolation (solar-only) and when coupled with other forcings (solar-residual). For the former we compare the early century solar-residual changes with the late century GHG + sulfate changes. This choice is dictated partly by the need to maximize the response signals. We realize that the solar-residual case may include some longwave forcing as part of the feedback mechanism that appears to amplify the response to solar when it is combined with other forcings. We also realize that the GHG + sulfate case includes some shortwave forcing, but note that this is small in the tropical regions, which are our main concern. The results we obtain here may warrant clarification using idealized forcing experiments.

To examine the geographical distribution of these changes, Figs. 6 and 7 show precipitation changes for two of the major Northern Hemisphere monsoon systems, the West African (Fig. 6) and South Asian monsoon (Fig. 7). Stippling on the figures indicates areas where the ensemble mean divided by the intraensemble standard deviation is greater than 1.0. The contour indicates areas where the ensemble mean difference is significant at the 10% level taken from a measure of variance in the control run over 50 years and assuming that to a first order the variance in each period is similar.

For the early century solar-only and GHG + sulfate, there are few areas of either consistent or significant model response in the West African (Fig. 6a,b) or South Asian (Fig. 7a,b) monsoon regions. One area of precipitation increase in the tropical Indian Ocean in the early century solar-only (Fig. 7a) is significant, but the precipitation index averaged over the entire monsoon region in Fig. 7a shows values near zero. However, for the early century solar-residual South Asian monsoon in Fig. 7c, there are a number of areas that are both consistent and significant in the tropical Indian Ocean and in northeastern India and south China with anomalies of greater than 1 mm day^{-1}. Many of the precipitation increases over the West African monsoon land areas for early century solar-residual (Fig. 6c) are nearly that size and are both consistent and significant. There is also a large positive increase of area-averaged precipitation of $+0.18$ mm day^{-1} for both the West African monsoon and South Asian monsoon for early century solar-residual (Figs. 6c and 7c, respectively). In contrast, though there are increases of precipitation over many areas of the West African and South Asian monsoons for late century GHG + sulfates (Figs. 6d and 7d), most are neither consistent across ensemble members or sig-

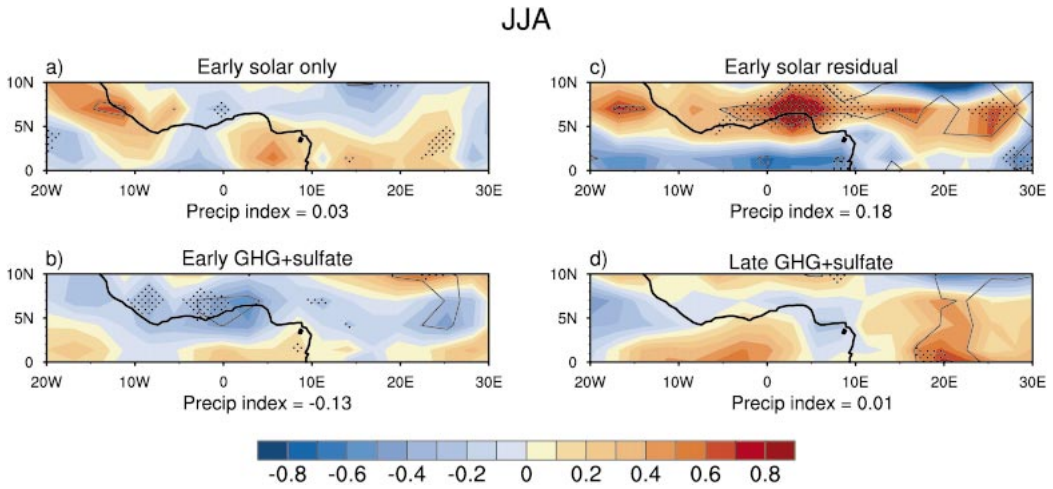

FIG. 6. (a) Precipitation differences (mm day^{-1}) for the early century solar-only for the West African monsoon region; precipitation index is area-averaged precipitation for 5°–10°N, 10°W–10°E; (b) same as (a) except for the early century GHG + sulfate; (c) same as (a) except for the early century solar residual; (d) same as (a) except for the late century GHG + sulfates. Stippling indicates regions where the ensemble mean divided by the intraensemble std dev exceeds 1.0; solid black contour shows areas where significance of differences exceeds the 10% level.

nificant, with area-averaged precipitation increases near zero.

Taken together, Fig. 7 shows that, for the South Asian monsoon, the greatest contribution to positive trends in monsoon precipitation arises from the addition of solar forcing to GHG + sulfates in the early century compared to the late century. Observations of monsoon precipitation can be used to check if there were greater positive trends in monsoon precipitation in the early compared to the late century as indicated by the model ensemble mean results. For a long-term index of observed monsoon rainfall we use the all-India monsoon rainfall index (Parthasarathy et al. 1991). The linear trend for the early century (1900–45) monsoon rainfall is +1.48 mm yr^{-1}. The midcentury linear trend (1945–60) is −0.80 mm yr^{-1} and the late century linear trend (1960–2000) is −0.10 mm yr^{-1}. Thus, the early century increase is greater than for the late century. This is qualitatively consistent with the results in Fig. 7, though we do not include black carbon (soot) over South Asia, which may be an important forcing in that region (Podgorny et al. 2000). Additionally, an analysis of observed precipitation trends in the IPCC Third Assessment report indicates that the early century precipitation trends over the South Asian monsoon region were mostly positive and larger than the late century trends in those regions (Folland et al. 2001), consistent with the Parthasarathy record and the results in Fig. 7.

It was noted earlier that changes in surface radiation could influence the monsoon through changes in meridional temperature gradient between Asia and the Indian Ocean. Though the details of the meridional temperature gradient are quite complicated in regards to regional changes of monsoon precipitation patterns (e.g., Meehl and Arblaster 2002a), a rough index for representing how north–south temperature contrast can influence the monsoon provided by that study is the surface temperature difference from central Asia to the Indian Ocean. For the South Asian monsoon, there is little meridional temperature gradient enhancement for early century solar-only or GHG + sulfates, consistent with the weak changes in monsoon precipitation in Fig. 7. The change in JJA surface temperature difference from central Asia to the tropical Indian Ocean is about +0.80°C for the early century solar-residual forcing ensemble, while for the late century GHG + sulfates the difference is almost half that at +0.45°C (not shown). However, these relatively small meridional temperature gradient enhancements are during the height of the monsoon. The gradients that set the stage for monsoon precipitation anomalies appear the previous winter and spring (e.g., Meehl 1997). For the early century solar-residual, the warming ranges from values greater than +1.75°C in central Asia to near zero in the tropical Indian Ocean for a meridional temperature gradient enhancement of about +1.75°C in DJF (not shown). For the late century GHG + sulfate, the DJF central Asian warming is mostly less than +1°C while the Indian Ocean warms on the order of +0.3°C, a gradient enhancement of around +0.7°C. Thus, there is more than a factor of 2 greater early century enhancement in the gradient for the solar-residual. This is reflected by the precipitation index increase in Fig. 7 of 0.18 mm day^{-1}.

Analysis of observations shows that, for strong minus weak monsoon years, there is a meridional surface temperature gradient increase between the northern Indian Ocean and central Asia of about 1.5°C in seasons prior to the monsoon (Meehl and Arblaster 2002a,b). Such a strengthened meridional temperature gradient here contributes to enhancements in South Asian monsoon rain-

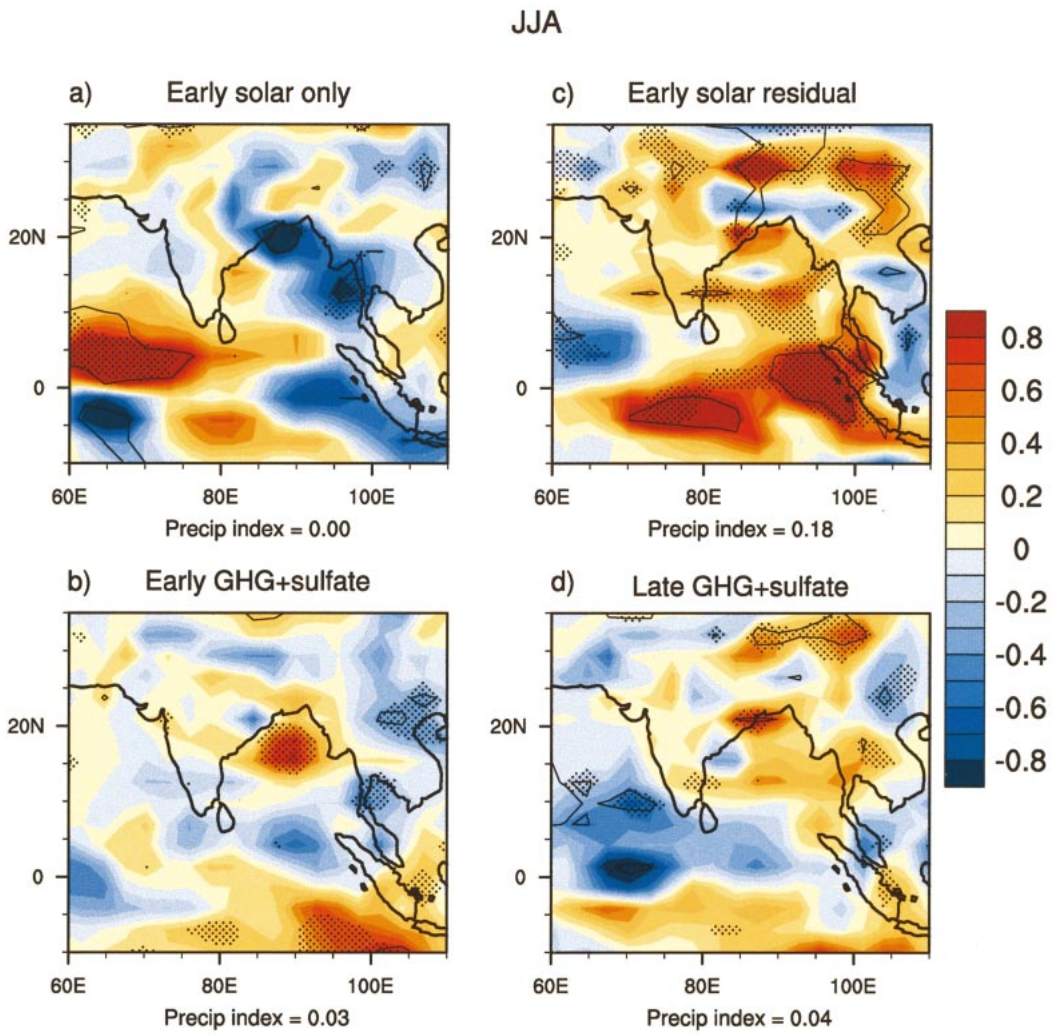

FIG. 7. Same as Fig. 6 except for the South Asian monsoon region; the precipitation index is the area-averaged precipitation for 10°S–35°N, 60°–110°E.

fall in the early century solar-residual compared to the early century solar-only. It was earlier noted (Fig. 5) that there was a factor of 2 or more increase in the net solar in the northern Tropics during DJF for the early century solar-residual ensemble mean compared to the late century ensembles with the largest values locally over Asia (not shown). This contributes to the enhanced meridional temperature gradients and greater south Asian monsoon rainfall.

For the West African monsoon, there are several competing mechanisms such as changes in land–ocean temperature gradient, warmer SSTs in the tropical Atlantic, and nonlinear feedback mechanisms. In the early century solar-residual ensembles, there is a slightly enhanced meridional temperature gradient in JJA (not shown), with warming over northern Africa of about +0.3°C and near-zero warming in the tropical Atlantic, but little enhancement in the solar-only. This would contribute to greater West African monsoon rainfall in the solar-residual case in Fig. 6. In the late century temperature differences for GHG + sulfates, there is almost uniform surface temperature warming from North Africa to the tropical Atlantic of about +0.30° to +0.40°C (not shown), thus providing little enhancement of meridional temperature gradient. The warmer SSTs in the southern tropical Atlantic in the late century would also contribute to a weaker monsoon over land (e.g., as noted in observations and a modeling study by, e.g., Folland et al. 1986) with positive precipitation anomalies of up to +0.4 mm day^{-1} near 10°S over ocean.

For DJF precipitation changes, regions that show large increases of precipitation for the early century are in the tropical eastern Indian, Indonesian/northern Australian, and western Pacific Ocean areas for both the solar-only and solar-residual (Figs. 8a,c). For the latter, there are consistent and statistically significant increases of about +1.5 mm day^{-1}. For the solar-only the anomalies are about half that magnitude and are neither con-

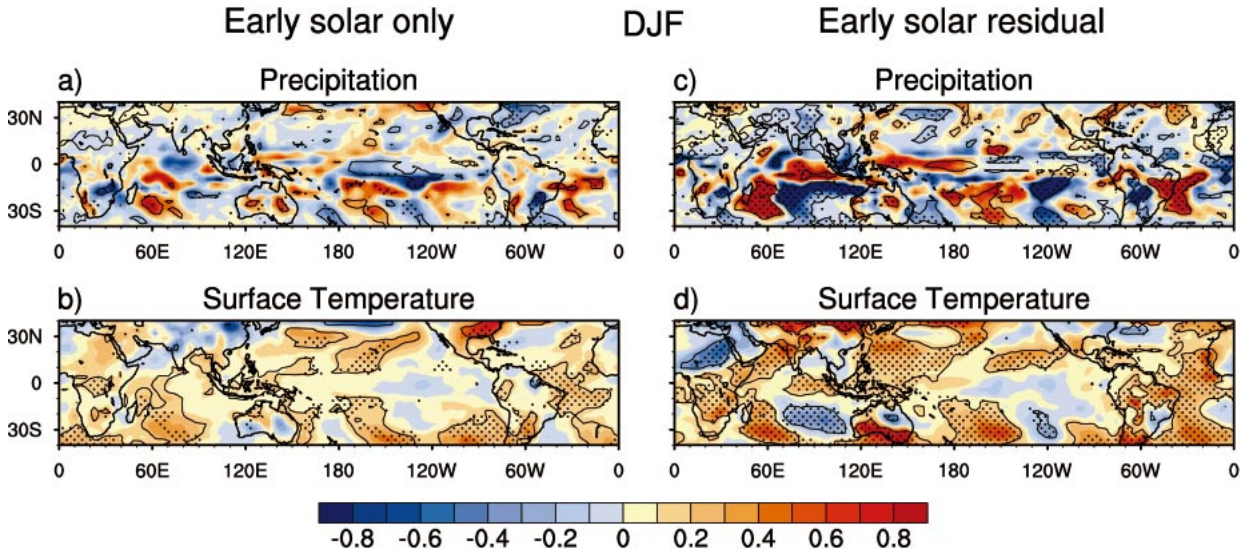

FIG. 8. (a) Precipitation anomalies (mm day^{-1}), DJF, the early twentieth-century solar-only; (b) same as (a) except for surface temperature (°C); (c) same as (a) except for the early century solar-residual; (d) same as (b) except for the early century solar-residual. Stippling indicates regions where the ensemble mean divided by the intraensemble std dev exceeds 1.0; solid black contour shows areas where significance of differences exceeds the 10% level.

sistent nor significant. There are also precipitation increases in DJF near 20°–30°S (Figs. 8a,c) for both the early century solar-residual and solar-only. These increases come mainly from enhanced precipitation in the South Indian convergence zone near Madagascar, the South Pacific convergence zone around and southeast of Fiji, and the South Atlantic convergence zone southeast of South America. Increases locally are greater for the early century solar-residual (Fig. 8c) compared to the solar-only (Fig. 8a). They are also greater for the late (Fig. 9c) relative to the early century (Fig. 9a) GHG + sulfates. In both cases, the increase is about a factor of 2 (about +1 mm day^{-1}), and the increases are both consistent and statistically significant.

Figure 10 shows area-averaged DJF precipitation values for the general regions of precipitation increase discussed above and compares precipitation changes for the early and late century periods. As indicated from the geographical plots in Figs. 8 and 9, the early century solar-residual area-averaged precipitation increases are greater than the early century solar-only values, with largest solar-residual increases of about 0.8 mm day^{-1} for the South Atlantic region. This increase is more than a factor of 2 greater than the intraensemble standard

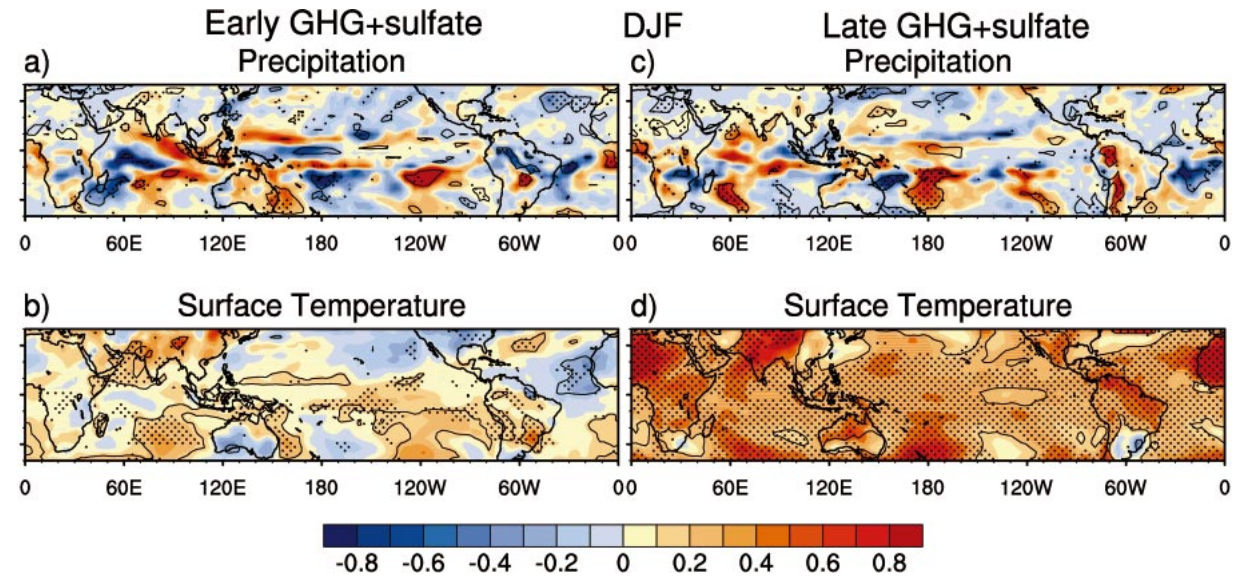

FIG. 9. Same as Fig. 8 except for (a), (b) the early century GHG + sulfates and (c), (d) the late century GHG + sulfates.

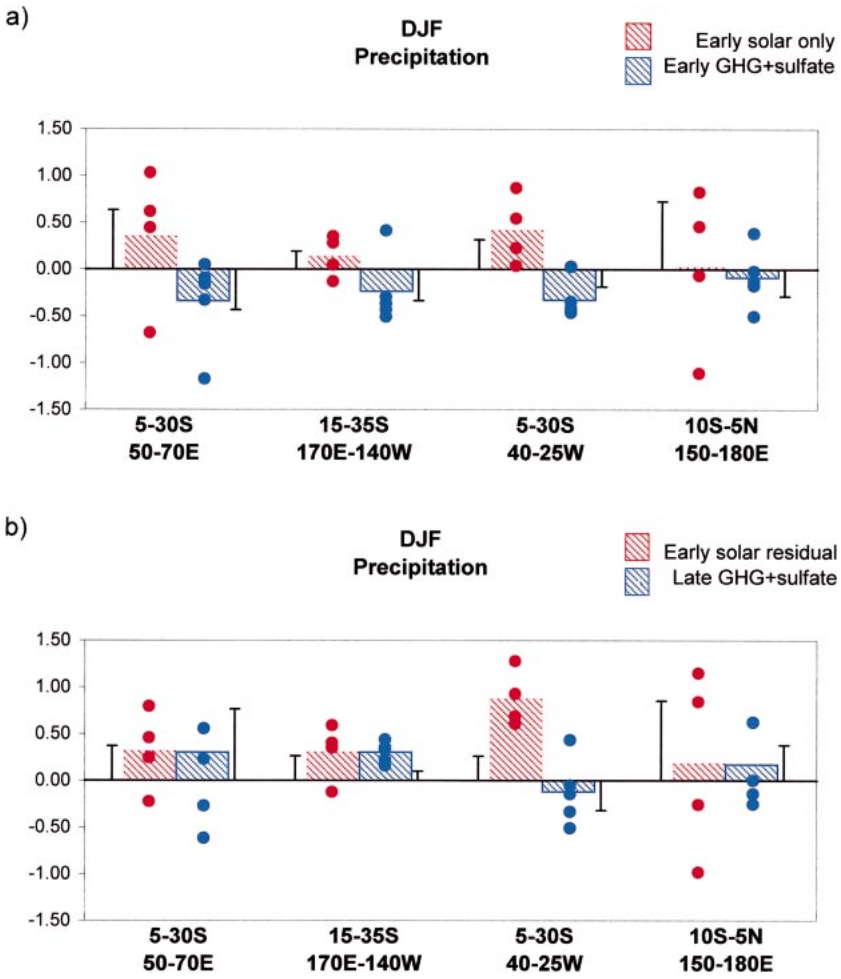

FIG. 10. (a) Area averages of DJF precipitation (mm day^{-1}) for, left to right, the South Indian convergence zone, South Pacific convergence zone, South Atlantic convergence zone, and tropical western Pacific (areas given in the figure) for the early century solar-only (red hatching) and the early century GHG + sulfates (blue hatching); (b) same as (a) except for the early century solar-residual (red hatching) and the late century GHG + sulfates (blue hatching). Bars show ensemble means, dots indicate individual ensemble member values, and thin black lines show intraensemble std dev.

deviation (and equal about one standard deviation from 300 years of control run simulation, not shown). Early century GHG + sulfates in Fig. 10 show small precipitation declines (probably not significant). Three out of four areas show precipitation increases for late century GHG + sulfates.

We noted above that, in DJF, late century GHG + sulfates tropical precipitation changes were much smaller in some areas of the Tropics compared to the early century solar-residual changes. The reason for these relative regional precipitation changes can be traced to areas upstream of the tropical convergence zones where the various forcings show different changes in the surface energy balance associated with the low-level moisture divergence (not shown). Here we choose these upstream areas for further analysis. The areas are characterized by patterns of low-level moisture divergence, which subsequently provide low-level moisture sources for the ocean convergence zones where there is enhanced precipitation. These areas include the tropical north and south Indian Ocean where surface divergence provides moisture for anomalous precipitation enhancement areas in the eastern equatorial Indian Ocean and South Indian convergence zone; a region south and west of Hawaii that provides moisture divergence for enhanced precipitation in the western tropical Pacific; an area in the South Pacific that supplies moisture for the South Pacific convergence zone; and an area in the tropical Atlantic upstream of the South Atlantic convergence zone. The area boundaries are defined in Figs. 11 and 12. The areas differ slightly between the solar-residual and solar-only cases due to somewhat different areas of maximum low-level moisture divergence in the respective ensemble means.

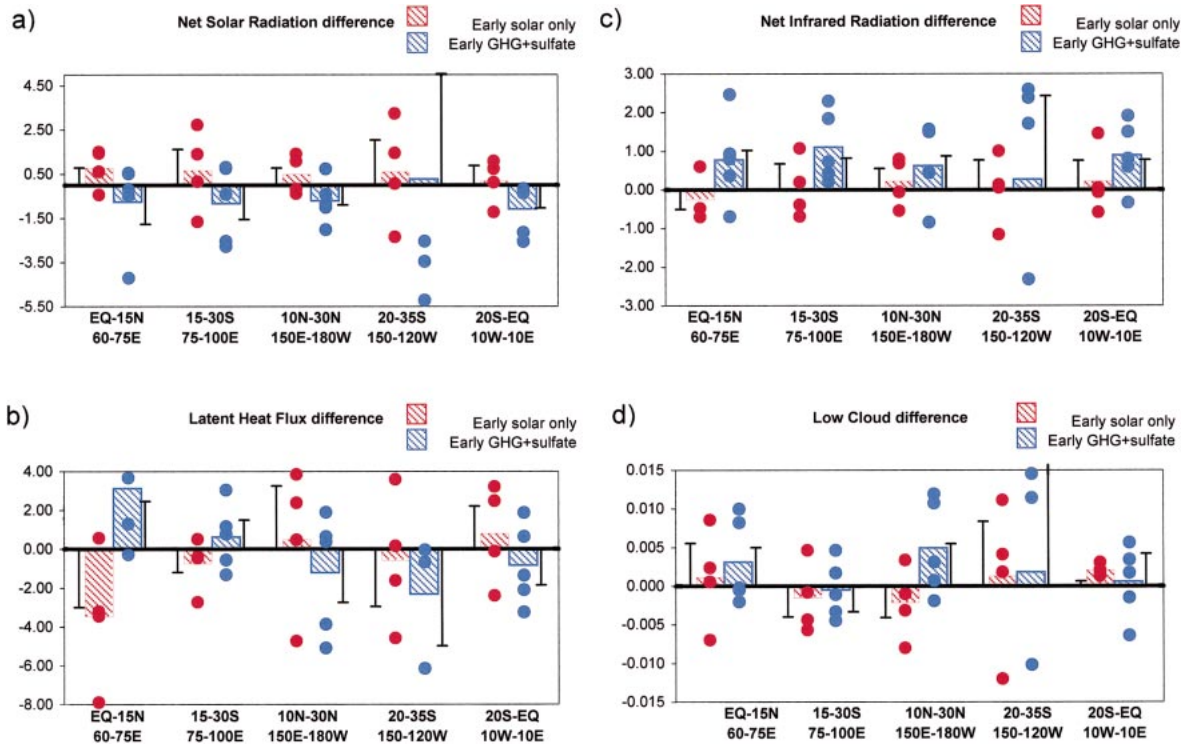

FIG. 11. (a) Area-averaged net solar radiation (W m^{-2}) for five areas denoting ocean low-level moisture divergence maxima (areas specified in panel) that serve as collection areas for low-level moisture carried to the tropical convergence zones, for the early century solar only (red hatching), and the early century GHG + sulfates (blue hatching); (b) same as (a) except for latent heat flux (W m^{-2}); (c) same as (a) except for net IR [values in (a), (b), and (c) that are positive denote energy input to the surface]; (d) same as (a) except for the low cloud fraction. Bars show ensemble means, dots indicate individual ensemble member values, and thin black lines show intraensemble std dev.

For net solar radiation from the early century period for the solar-only (Fig. 11a) and solar-residual cases (Fig. 12a) all areas show positive anomalies, though solar-residual values are 30% to a factor of 4 larger than the solar-only values. In almost all cases, the signals are smaller than, or comparable to, the intraensemble and natural (control run) standard deviations. The consistency across regions, however, indicates the presence of a physically meaningful effect.

The increase of solar energy at the surface should increase the latent heat flux to maintain a surface energy balance. Three of the five areas for the early century solar-only (Fig. 11b) show negative anomalies indicating increased latent heat flux removed from the surface. The anomalies, however, are not significant relative to the two noise criteria, except perhaps for the Arabian Sea area. Early century solar-residual latent heat flux differences are negative for all five areas indicating that more energy is removed from the surface by evaporation. This amplification is consistent with the net solar-radiation amplification, although we note that none of the changes is highly significant except for perhaps the southern tropical Indian Ocean. The greater low-level moisture source associated with these increases in latent heat flux then provides more moisture for advection into the areas of low-level moisture convergence, thus contributing to the positive precipitation anomalies shown in Figs. 8a,c, and 10. The larger and more consistent negative latent heat flux anomalies in the solar-residual case are consistent with the greater positive precipitation anomalies in the oceanic convergence zones that occur in this case. Note too that the enhanced latent heat removal from the surface in the low-level moisture divergence regions is associated with consistent and significant regional SST decreases, and that there are corresponding increases in SST in areas of precipitation increase (Fig. 8d).

These ocean–atmosphere interactions are further amplified by cloud changes. As precipitation increases in the oceanic convergence zones, there is increased upward vertical motion over the positive precipitation anomalies, and enhanced subsidence over areas of low-level moisture divergence. This produces decreases of low cloud in four out of five areas in Fig. 12d for the early century solar-residual case, though we note again that signal-to-noise levels are small. There are two areas with negative low cloud changes for the early century solar-only in Fig. 11d (south Indian and western Pacific).

For the GHG + sulfates cases, greater amounts of CO_2 and other GHGs should increase downward infrared radiation, as is the case in both Figs. 11c and 12c. Late century values are larger and more consistent as-

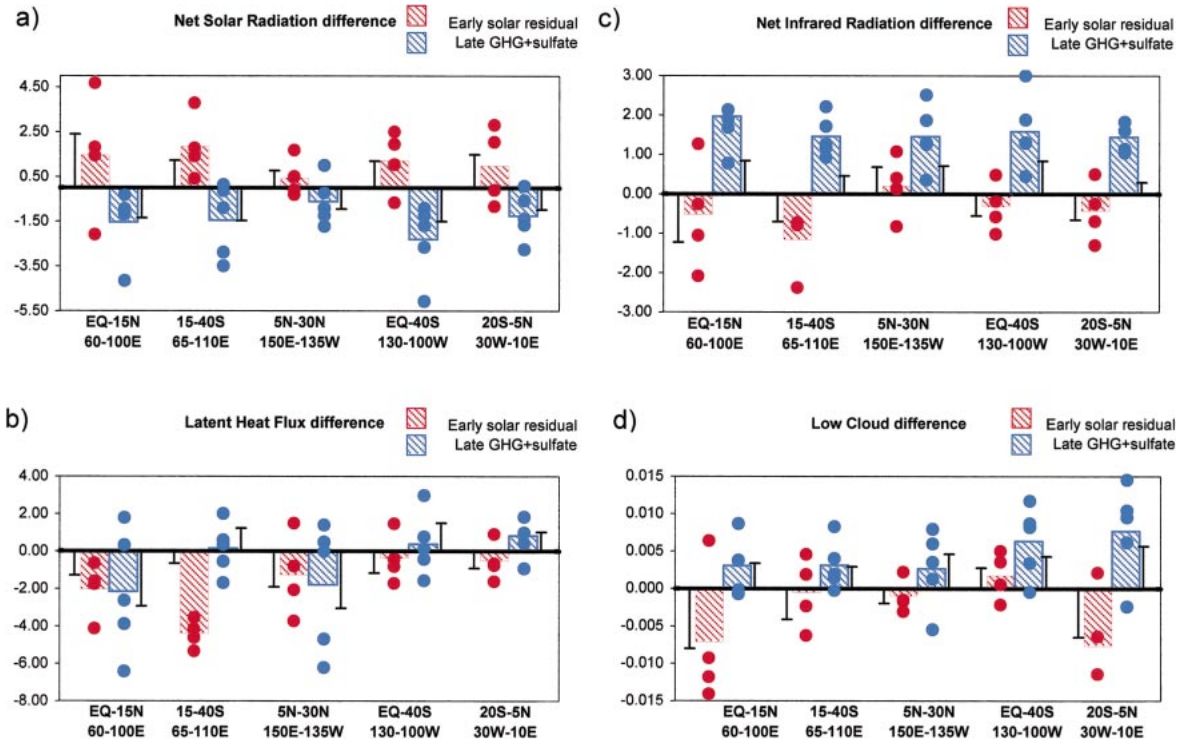

FIG. 12. Same as Fig. 11 except for the early century solar-residual (red hatching) and the late century GHG + sulfates (blue hatching).

sociated with the greater forcing. Since GHG IR forcing is relatively spatially uniform, there are increases in downward IR at most locations (not shown) that produce more spatially uniform, consistent, and significant increases of SST, especially for the late century period in Fig. 9d. This SST increase contributes to an enhanced supply of low-level moisture, in turn, leading to increases in low cloud for four out of five areas for the early century and all five areas in the late century. All but two for the latter exceed one intraensemble standard deviation. This increase in low cloud then contributes to a decrease in the net solar radiation in four out of five areas for the early century in Fig. 11a, and all five areas in Fig. 12a for the late century. The end result is a weak and inconsistent response of latent heat flux for most areas in Figs. 11b and 12b in the area averages (though spatially localized increases of latent heat removed from the surface contribute to the increases in low cloud, not shown).

6. Discussion

We have identified two sets of processes that lead to differential monsoon and ocean convergence zone responses to shortwave and longwave forcing, and to an apparent nonlinear amplification of the response to solar forcing. The fundamental difference is that solar forcing is more spatially heterogeneous (i.e., acting most strongly in areas where sunlight reaches the surface), while greenhouse gas forcing is more spatially uniform. Consequently, solar forcing produces feedbacks involving temperature gradient–driven regional circulation regimes (e.g., Lindzen and Nigam 1987) that can alter clouds. Over relatively cloud-free oceanic regions in the subtropics, in areas of low-level moisture divergence (the moisture source areas for the ocean precipitation convergence zones), the enhanced solar heating produces greater evaporation. This increased moisture then converges into the precipitation zones, intensifying the upward vertical motions of the regional Hadley and Walker circulations. The subsidence associated with this enhanced regional vertical motion results in less low clouds over the subtropical ocean regions, allowing even more solar energy to reach the surface, and so on.

Since the greenhouse gas forcing is more spatially uniform, such regional circulation feedbacks are not as strong. Warmer SSTs and associated low cloud increases are not as spatially differentiated, SST gradient–driven circulations do not set up, and the convergence zone precipitation regimes are not intensified in the same way as for the solar-forcing cases. The response for GHG + sulfates for the early and late century are proportional to the strength of the forcing, with a larger response for the greater late century forcing.

For GHG + sulfates forcing, most of the factors (including precipitation changes) show larger magnitude trends in the late century, when the forcing is larger, than in the early century. For solar forcing, however, some form of nonlinear mechanism appears to be acting in the model. When considered as a residual from an-

thropogenic plus solar relative to pure anthropogenic forcing, the solar effects are substantially larger than when solar forcing is considered alone. (We examined only the early century period in this regard, because this period has a larger ''base level'' solar forcing trend than the late century period.) This nonlinear interaction can be traced to the increase of SST of +0.2° to +0.3°C in the regions of low-level moisture divergence produced by the GHG + sulfates forcing seen in Fig. 9b. When solar forcing is added to these base-state SST changes, the regional feedbacks are more intense and produce a greater response in the early century solar-residual compared to the solar-only. Increases of comparable magnitude in the tropical Atlantic and Indian Oceans during JJA contribute similarly to intensification of the monsoon regimes in these regions. While none of the regions exhibits highly significant changes, the regional consistency of the mechanisms supports their general validity in the model.

To give an example of how such relatively small increases of tropical SSTs can produce changes in tropical precipitation, Meehl and Arblaster (2002a) increased climatological tropical Indian Ocean SSTs by 0.75°C north of 15°S and ran an ensemble of five members with specified climatological SSTs elsewhere. The result was statistically significant precipitation anomalies of +1 to +3 mm day^{-1} over much of western, northern, and northeastern India as well as over the tropical Indian Ocean. An area-averaged Indian monsoon index (all points 5°–40°N, 60°–100°E) for JJA showed an increase of about five standard deviations showing that higher Indian Ocean SSTs in increments of less than 1°C can, by themselves, intensify the Indian monsoon and, by implication, other convergence-related precipitation regimes such as the DJF oceanic convergence zones.

Though we are examining these model responses to transient forcings, the nature of the mechanisms involving regional coupled interactions and tropical rainfall should more generally hold for an equilibrium state. Further experiments with a fully coupled model run to equilibrium separately with different forcings would be required to address this issue.

7. Conclusions

We performed ensembles of global coupled climate model experiments, four runs with solar + GHG + sulfates (with changes in tropospheric and stratospheric ozone as well), four runs including only the time evolution of solar forcing, and five runs with only GHG + sulfates (with changes in tropospheric and stratospheric ozone). The difference between solar + GHG + sulfates minus GHG + sulfates is the response to the solar forcing as a residual. The climate changes for the early century and late century periods are evaluated for consistency among the ensemble members: if the ensemble mean change divided by the intraensemble standard deviation is greater than one, the ensemble mean difference is denoted as a consistent response (e.g., Cubasch et al. 2001). We also assessed the significance of changes based on interannual control run standard deviations (using a 50-yr period, comparable in length to the periods evaluated in the perturbation experiments).

It has been observed that globally averaged warming of surface air temperature in the twentieth century occurred in two stages, early in the century from about the early 1900s to the 1940s, and late in the century from about the late 1960s to 2000 (Fig. 1b). Previous work suggests that it is likely that the early century warming was caused mostly by solar and volcanic forcing, and the late century warming mostly by the increase of greenhouse gases (partially offset by aerosol cooling). These results are confirmed here. Such confirmation, however, is not the main purpose of this paper. Rather, our focus is on the seasonal and regional nature of the two different types of forcing and response, solar in the early century period and GHG + sulfates in the late century period.

An analysis of surface energy balance shows a large land–ocean forcing differential (primarily due to solar forcing) in both DJF and JJA in the early period (especially in the solar-residual results), but no large differential in the later period when the dominant forcing is infrared radiation. As a partial consequence, the ratio of land to ocean warming is 2.6 and 2.7 in DJF and JJA, respectively, for the early century solar-residual, while the land–ocean warming ratio is only 1.5 and 1.3 in DJF and JJA, respectively, for the late century GHG + sulfates. The smaller land–ocean heating ratio is partly related to the diurnal cycle. Solar forcing occurs only during the day and is greatest in clear-sky areas. Over the oceans this excess energy is used to evaporate moisture from the surface and, thus, there is less heating over the ocean than over land. In contrast, the IR forcing occurs more uniformly during day and night. There is, thus, proportionately less energy available for evaporation and this results in a warmer ocean surface and a smaller land–ocean warming ratio.

Of particular interest is the transient climate system response in the early and late twentieth century when the nature of the forcing was fundamentally different. Solar forcing is more spatially heterogeneous (i.e., acting most strongly in areas where sunlight reaches the surface) while greenhouse gas forcing is more spatially uniform. Consequently, solar forcing induces feedbacks involving temperature gradient–driven circulation regimes that can alter clouds. Over relatively cloud-free oceanic regions of low-level moisture divergence in the subtropics (i.e., the moisture collection areas the feed the oceanic and monsoon precipitation maxima), the enhanced solar forcing produces greater evaporation. More moisture then converges into the precipitation zones, intensifying the regional monsoon and Hadley and Walker circulations. This produces greater subsidence and less clouds over the subtropical ocean regions, and even more solar forcing. Since the green-

house gases are more spatially uniform, such regional circulation feedbacks are not as strong.

These coupled regional responses are most evident when the solar forcing occurs in concert with increased greenhouse gas forcing of about the same magnitude in the early twentieth century (the latter raises the base-state tropical SSTs to fuel the regional feedbacks induced by the spatially differentiated solar forcing). There are two consequences of this. The first is an amplified solar response in the early century, in which, even though the early century GHG + sulfate forcing is less than in the late century, the overall effect on monsoon precipitation is larger in the early century period (by a factor of 2 to nearly an order of magnitude). A similar effect occurs in the tropical Pacific and in the Southern Ocean convergence zones.

Linear trends calculated from the observed all-india monsoon rainfall index show that monsoon rainfall increased more in the early century compared to the late century, consistent with the above finding. The early century increase in our model results is associated with enhanced solar forcing. Though we cannot definitively attribute these observed changes in Indian monsoon precipitation to solar forcing, the observational results are qualitatively consistent with the model results. It is important to repeat these experiments with a more realistic forcing such as black carbon (soot), and to also consider the indirect forcing effects of sulfate aerosols.

Thus, the model results show that the very nature of the different forcings (solar and IR) produces different responses in the coupled climate system. The nonlinear interaction in the early century between the solar and GHG forcing intensifies the tropical precipitation response. More details regarding the nature of the amplification of the solar forcing in early twentieth century will be the subject of a subsequent study.

Acknowledgments. The authors thank Harry van Loon for stimulating discussions and comments, and David Rind and an anonymous reviewer for insightful comments. A portion of this study was supported by the Office of Biological and Environmental Research, U.S. Department of Energy, as part of its Climate Change Prediction Program, and by NOAA Office of Global Programs under Grant NA87GO0105(TMLW).

REFERENCES

Balachandran, N. K., D. Rind, P. Lonergan, and D. R. Shindell, 1999: Effects of solar cycle variability on the lower stratosphere and the troposphere. *J. Geophys. Res.,* **104,** 27 321–27 339.

Bonan, G. B., 1998: The land surface climatology of the NCAR land surface model (LSM 1.0) couplet to the NCAR Community Climate Model (CCM3). *J. Climate,* **11,** 1307–1326.

Crowley, T. J., 2000: Causes of climate change over the past 1000 years. *Science,* **289,** 270–277.

Cubasch, U., R. Voss, G. C. Hegerl, J. Waszkewitz, and T. J. Crowley, 1997: Simulation of the influence of solar radiation variations on the global climate with an ocean–atmosphere general circulation model. *Climate Dyn.,* **13,** 757–767.

——, and Coauthors, 2001: Projections of future climate change. *Climate Change 2001: The Scientific Basis,* J. T. Houghton et al., Eds., Cambridge University Press, 525–582.

Dai, A., G. A. Meehl, W. M. Washington, and T. M. L. Wigley, 2001a: Ensemble simulations of twenty-first-century climate changes: Business as usual versus CO_2 stabilization. *Bull. Amer. Meteor. Soc.,* **82,** 2377–2388.

——, T. M. L. Wigley, B. A. Boville, J. T. Kiehl, and L. E. Buja, 2001b: Climates of twentieth and twenty-first centuries simulated by the NCAR Climate System Model. *J. Climate,* **14,** 485–519.

——, ——, G. A. Meehl, and W. M. Washington, 2001c: Effects of stabilizing atmospheric CO_2 on global climate in the next two centuries. *Geophys. Res. Lett.,* **28,** 4511–4514.

Delworth, T. L., and T. R. Knutson, 2000: Simulation of the early 20th century global warming. *Science,* **287,** 2246–2250.

Folland, C. K., T. N. Palmer, and D. E. Parker, 1986: Sahel rainfall and worldwide sea temperature. *Nature,* **320,** 602–607.

——, and Coauthors, 2001: Observed climate variability and change. *Climage Change 2001: The Scientific Basis,* J. T. Houghton et al., Eds., Cambridge University Press, 99–181.

Haigh, J. D., 1996: The impact of solar variability on climate. *Science,* **272,** 981–984.

Hansen, J., A. Lacis, D. Rind, G. Russell, P. Stone, I. Fung, R. Ruedy, and J. Lerner, 1984: Climate sensitivity: Analysis of feedback mechanisms. *Climate Processes and Climate Sensitivity, Geophys. Monogr.,* No. 29, Amer. Geophys. Union, 130–163.

Hoyt, D. V., and K. H. Schatten, 1993: A discussion of plausible solar irradiance variations, 1700–1992. *J. Geophys. Res.,* **98,** 18 895–18 906.

Jones, P. D., M. New, D. E. Parker, S. Martin, and I. G. Rigor, 1999: Surface air temperature and its changes over the past 150 years. *Rev. Geophys.,* **37,** 173–199.

Joussaume, S., and Coauthors, 1999: Monsoon changes for 6000 years ago: Results of 18 simulations from the Paleoclimate Modeling Intercomparison Project (PMIP). *Geophys. Res. Lett.,* **26,** 859–862.

Kiehl, J. T., and B. P. Briegleb, 1993: The relative roles of sulfate aerosols and greenhouse gases in climate forcing. *Science,* **260,** 311–314.

——, J. J. Hack, G. Bonan, B. Boville, D. Williamson, and P. Rasch, 1998: The National Center for Atmospheric Research Community Climate Model (CCM3). *J. Climate,* **11,** 1131–1149.

Kutzbach, J., R. Gallimore, S. Harrison, P. Behling, R. Selin, and F. Laarif, 1998: Climate and biome simulations for the past 21,000 years. *Quat. Sci. Rev.,* **17,** 473–506.

Labitzke, K., and H. van Loon, 1995: Connection between the troposphere and stratosphere on a decadal scale. *Tellus,* **47A,** 275–286.

Lean, J., and D. Rind, 1998: Climate forcing by changing solar radiation. *J. Climate,* **11,** 3069–3094.

——, J. Beer, and R. Bradley, 1995: Reconstruction of solar irradiance since 1610: Implications for climate change. *Geophys. Res. Lett.,* **22,** 3195–3198.

Lindzen, R. S., and S. Nigam, 1987: On the role of sea surface temperature gradients in forcing low level winds and convergence in the tropics. *J. Atmos. Sci.,* **44,** 2418–2436.

Mann, M. E., R. S. Bradley, and M. D. Hughes, 1998: Global-scale temperature patterns and climate forcing over the past six centuries. *Nature,* **392,** 779–787.

Meehl, G. A., 1997: The south Asian monsoon and the tropospheric biennial oscillation. *J. Climate,* **10,** 1921–1943.

——, and J. M. Arblaster, 2002a: GCM sensitivity experiments for the Indian monsoon and tropospheric biennial oscillation transition conditions. *J. Climate,* **15,** 923–944.

——, and ——, 2002b: The tropospheric biennial oscillation and Asian–Australian monsoon rainfall. *J. Climate,* **15,** 722–744.

——, W. M. Washington, D. J. Erickson III, B. P. Briegleb, and P. J. Jaumann, 1996: Climate change from increased CO_2 and the direct and indirect effects of sulfate aerosols. *Geophys. Res. Lett.,* **23,** 3755–3758.

——, W. D. Collins, B. Boville, J. T. Kiehl, T. M. L. Wigley, and J. M. Arblaster, 2000: Response of the NCAR Climate System Model to increased CO_2 and the role of physical processes. *J. Climate*, **13,** 1879–1898.

——, P. Gent, J. M. Arblaster, B. Otto-Bliesner, E. Brady, and A. Craig, 2001: Factors that affect amplitude of El Niño in global coupled climate models. *Climate Dyn.,* **17,** 515–526.

Parthasarathy, B., K. Rupa Kumar, and A. A. Munot, 1991: Evidence of secular variations in Indian monsoon rainfall–circulation relationships. *J. Climate*, **4,** 927–938.

Podgorny, I. A., W. Conant, V. Ramanathan, and S. K. Satheesh, 2000: Aerosol modulation of atmospheric and surface solar heating over the tropical Indian Ocean. *Tellus*, **52B,** 947–958.

Rind, D., and N. K. Balachandran, 1995: Modelling the effects of UV variability and the QBO on the troposphere–stratosphere system. Part II: The troposphere. *J. Climate*, **8,** 2080–2095.

——, J. Lean, and R. Healy, 1999: Simulated time-dependent climate response to solar radiative forcing since 1600. *J. Geophys. Res.,* **104,** 1973–1990.

Shindell, D., D. Rind, N. Balachandran, J. U. Lean, and P. Lonergan, 1999: Solar cycle variability, ozone, and climate. *Science*, **284,** 305–308.

——, G. A. Schmidt, R. L. Miller, and D. Rind, 2001: Northern hemisphere winter climate response to greenhouse gas, ozone, solar, and volcanic forcing. *J. Geophys. Res.,* **106,** 7193–7210.

Smith, R. L., T. M. L. Wigley, and B. D. Santer, 2003: A bivariate time series approach to anthropogenic trend detection in hemispheric mean temperatures. *J. Climate*, in press.

Stott, P. A., S. F. B. Tett, G. S. Jones, M. R. Allen, J. F. B. Mitchell, and G. J. Jenkins, 2000: External control of 20th century temperature by natural and anthropogenic forcings. *Science*, **290,** 2133–2137.

——, ——, ——, ——, W. J. Ingram, and J. F. B. Mitchell, 2001: Attribution of twentieth century temperature change to natural and anthropogenic causes. *Climate Dyn.,* **17,** 1–21.

van Loon, H., and K. Labitzke, 1994: The 10–12-year atmospheric oscillation. *Meteor. Z.,* **3,** 259–266.

——, and D. J. Shea, 2000: The global 11-year solar signal in July–August. *Geophys. Res. Lett.,* **27,** 2965–2968.

Waple, A. M., M. E. Mann, and R. S. Bradley, 2002: Long-term patterns of solar irradiance forcing in model experiments and proxy based surface temperature reconstructions. *Climate Dyn.,* **18,** 563–578.

Washington, W. M., and Coauthors, 2000: Parallel climate model (PCM) control and transient simulations. *Climate Dyn.,* **16,** 755–774.

Wetherald, R. T., and S. Manabe, 1975: The effects of changing the solar constant on the climate of a general circulation model. *J. Atmos. Sci.,* **32,** 2044–2059.

Wigley, T. M. L., P. D. Jones, and S. C. B. Raper, 1997: The observed global warming record: What does it tell us? *Proc. Nat. Acad. Sci. USA*, **94,** 8314–8320.